Original Article

Discrimination of dicentric chromosome from radiation exposure patient data using a pretrained deep learning model

Soon Woo Kwon [a,d], Won Il Jang [b], Mi-Sook Kim [b], Ki Moon Seong [a], Yang Hee Lee [a], Hyo Jin Yoon [a], Susan Yang [a], Younghyun Lee [c], Hyung Jin Shim [d,*]

[a] Lab of Biological Dosimetry, National Radiation Emergency Medical Center, Korea Institute of Radiological and Medical Sciences, 75 Nowon-ro, Nowon-gu, Seoul, Republic of Korea
[b] Radiation Oncology, Korea Cancer Center Hospital, Korea Institute of Radiological and Medical Sciences, 75 Nowon-ro, Nowon-gu, Seoul, Republic of Korea
[c] Department of Biomedical Laboratory Science, College of Medical Sciences, Soonchunhyang University, Asan, Republic of Korea
[d] Department of Nuclear Engineering, Seoul National University, Republic of Korea

A B S T R A C T

The dicentric chromosome assay is a gold standard method to estimate radiation exposure by calculating the ratio of dicentric chromosomes existing in cells. The objective of this study was to propose an automatic dicentric chromosome discrimination method based on deep convolutional neural networks using radiation exposure patient data. From 45 patients with radiation exposure, conventional Giemsa-stained images of 116,258 normal and 2800 dicentric chromosomes were confirmed. ImageNet was used to pre-train VGG19, which was modified and fine-tuned. The proposed modified VGG19 demonstrated dicentric chromosome discrimination performance, with a true positive rate of 0.927, a true negative rate of 0.997, a positive predictive value of 0.882, a negative predictive value of 0.998, and an area under the receiver operating characteristic curve of 0.997.

1. Introduction

Dicentric chromosomes (DCs), representing a type of chromosome aberration, are biomarkers of radiation dose estimation. The dicentric chromosome assay (DCA) is the gold standard method in biological dosimetry [1], in which the number of DCs is counted on among conventional Giemsa-stained metaphase cells. Trained experts can score 500 cells or 100 DCs on metaphase spread images, achieving reasonably accurate dose estimations according to the International Atomic Energy Agency (IAEA) DC scoring recommendation [1]. However, for each patient, this DC scoring method is known [1] to take two or three days. Therefore, to save scoring time, a number of attempts [2–10] to develop automated DCAs have been proposed.

The automated DCA process involves three main stages: metaphase spread identification, chromosome detection, and DC discrimination [11]. Scorable candidate metaphase images are selected from low-resolution scans of chromosome microscope slides in the first stage of metaphase spread identification. The chromosome detection stage aims to detect individual chromosomes from metaphase spread images that contain chromosomes and stains, and the DC discrimination stage distinguishes DCs and normal chromosomes among the individual chromosome images.

Several methods [2,7,12–17] based on machine learning techniques have been proposed for automatic DC discrimination. Lorch et al. [12] proposed a DC detection procedure that involves obtaining chromosome image skeletons with local maxima of digitized chromosome pixel value levels. Piper and Sprey [13] proposed an adaptive classifier to determine the number of centromeres per chromosome by measuring the number of local minima in longitudinal integrated density profiles of chromosomes. Schunck et al. [2] reported the performance of the Metafer DCScore, a commercial, automated DC scoring module. Furthermore, Romm et al. [14] compared the levels of performance of three Metafer DCScore-integrated classifiers for DC detection. Employing classification criteria, such as chromosome width, length, and area, these DCScore classifiers were modified at the Federal Office for Radiation Protection (Bundesamt für Strahlenschutz) in Germany and the Institute for Radiological Protection and Nuclear Safety (L'Institut de Radioprotection et de Sûreté Nucléaire) in France. Arachchige et al. [18]

proposed a centromere counting method that involves extracting centerlines with pruning skeletons based on discrete curve evolution [19]. In addition, Arachchige et al. [16] proposed an intensity-integrated Laplacian-based thickness measurement method to detect centromeres. Li et al. [17] developed a DC discrimination method using a support vector machine and a boosting classifier. Shen et al. [7] proposed a DC detection classifier using the widths and gray values of centromeres. However, these classical machine learning-based DC discrimination methods are limited in their accuracies, with true positive rates (TPRs) of 0.50–0.85 and positive predictive values (PPVs) of 0.44–0.83.

Deep learning (DL) technology [20–24] has recently shown outstanding performance in image analysis. In related research fields, the DL method has been actively applied to classify Giemsa-banded chromosomes for karyotyping [25–31]. In addition, Jang et al. [8] have successfully applied the DL method to identify DCs from ex vivo conventional Giemsa-stained chromosome images using the Faster Region-based Convolutional Network (Faster R–CNN) [32] with Feature Pyramid Networks (FPN) [33]. Moreover, Shen et al. used two-stage DL networks for DC identification [10].

The occurrence of DCs, which are sensitive to radiation exposure, is a rare event in nature. Hence, previous studies have been conducted on data gathered from irradiated ex vivo samples. However, this study aims to propose a high-precision automatic DC discrimination deep convolutional neural network (DCNN) that can employ DCs obtained in vivo from radiation exposure patients from the Korea Institute of Radiological Medical Sciences (KIRAMS). Moreover, we investigated the performance of our DCNN using mixed in vivo datasets from KIRAMS and ex vivo chromosome datasets from the Dongnam Institute of Radiological & Medical Sciences (DIRAMS) to show its applicability for DC discrimination on the different datasets.

2. Materials and methods

2.1. Preparation of in vivo chromosome images

In this study, 2868 metaphase spread images, each containing at least one DC, from 45 patients with radiation exposure from KIRAMS from 2010 to 2017 were selected to build the in vivo and KIRAMS datasets. The metaphase images were prepared from the patients' peripheral blood lymphocytes following the IAEA recommendation protocol [1]. The blood samples were incubated at 37.0 °C with 5% CO_2 for 24 h. After that, the lymphocytes were isolated and cultivated for 24 h in culture medium containing a mitotic inhibitor (0.06 μg/ml Colcemid; Gibco, KaryoMAX COLCEMID Solution, USA). Then, hypotonic potassium chloride treatment was used to harvest metaphase cells, which were fixed in a 3:1 mixture of methanol and acetic acid. The slides were dried at 60 °C for 20 h and stained using the solid Giemsa method. Finally, Metaphase images were obtained using the Metafer 4 systems (MetaSystems, Germany), equipped with a CoolCube 1 camera, which supports a resolution of 1360 x 1024 pixels and has a pixel size of 6.45 μm × 6.45 μm. The images were taken using Zeiss Axio Imager Z2 microscopes (Carl Zeiss, Germany) and with an objecitve Plan-Apochromat 63x/1.4 oil.

From the KIRAMS metaphase spread images, individual chromosome images were obtained by cropping rectangular-shaped fields along the contour of each chromosome edge. Then, a padding operation was applied to the rectangular images to change their proportions to square. The background of each cropped image was removed so that the target chromosome remained with its mask. The background pixel value was then filled with the average color of the pixels that had been removed so that the processed image had the appearance of the original on the metaphase image. The input images were resized to 64 × 64 pixels.

2.2. Training, validation, and test datasets

In addition to the in vivo chromosome images obtained from KIRAMS, ex vivo images were derived from the DIRAMS database [8], which has a number of DC and normal chromosome images. Table 1 shows the numbers of normal chromosomes and DCs among the in vivo and ex vivo datasets used for the training, validation, and testing of the DCNN models. Note that the chromosome numbers of the validation datasets for each label were set to approximately 10% of the sum of the training and validation numbers.

Fig. 1 shows examples of the chromosome images from the KIRAMS and DIRAMS datasets. As mentioned above, the DIRAMS datasets consist of ex vivo datasets obtained from blood irradiated using ^{60}Co gamma rays. Six different dose levels were used: 0, 0.5, 1, 2, 3, and 4 Gy. The radiation was delivered at an absorbed dose rate of 0.8 Gy/min, as measured by an ionization chamber detector [8]. Conversely, the KIRAMS datasets were derived from in vivo radiation exposure patient samples.

In addition to the KIRAMS and DIRAMS datasets, "Subsampled KIRAMS" and "KIRAMS + DIRAMS" datasets were prepared. Table 2 shows the numbers of normal chromosomes and DCs from those two datasets. In the subsampled KIRAMS datasets, the number of normal chromosomes for each label was adjusted to equal that of the DCs by random sampling. The KIRAMS + DIRAMS dataset was created simply by merging the two types of datasets. The test dataset was the KIRAMS test dataset.

2.3. Modified DCNN models for DC discrimination

This study used DCNNs to discriminate between individuals with normal chromosomes and DCs. DCNNs, DenseNet121, DenseNet201 [23], EfficientNetB5, EfficientNetB6 [24], ResNet101, ResNet152 [22], VGG16, and VGG19 [21] on Keras [34] were selected. As shown in Fig. 2, each DCNN without classifiers was utilized as a feature extractor. The classifier was modified with a global average or a max pooling layer, a dropout layer, and a batch normalization layer. The last layer of the classifier was set to the sigmoid layer for the binary classification. Random horizontal and vertical flips, random zooms with 0.1 ratios, and random rotation online augmentations were applied to the preprocessing layers before the DCNNs were modified to feed various input image shapes.

Furthermore, the transfer learning method was applied to train the DCNNs. The transfer learning method is a well-known method that enhances the performance of DCNNs trained on scarce data from a target domain using the weight of DCNNs trained on abundant data from a source domain. The weights of the pre-trained DCNNs on the publicly accessible ImageNet dataset [35] were fine-tuned for this DC discrimination task. Rescaling methods for fine-tuning the pre-trained DCNNs were applied with the origin rescaling method for the pre-trained DCNNs. Labels 0 and 1 indicate DCs and normal chromosomes, respectively.

2.4. Experimental setting

The training and testing were conducted on an Ubuntu 20.04 server with an Xeon® E5-2680 v4 CPU @ 2.40 GHz with 128 GB of RAM, and

Table 1
The number of chromosome images in training, validation, and test datasets of normal chromosomes and DCs from the KIRAMS and DIRAMS databases.

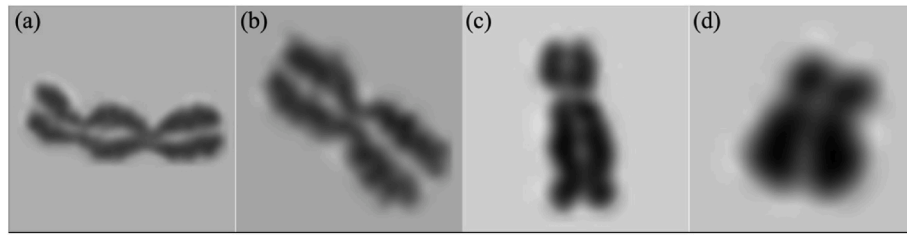|	KIRAMS dataset		DIRAMS dataset	
	Normal	Dicentric	Normal	Dicentric
Training	99,416	2397	13,506	9273
Validation	11,046	266	1501	1030
Test	5796	137	156	115

Fig. 1. (a) DC and (b) normal chromosome images from the KIRAMS dataset and (c) DC and (d) normal chromosome images from the DIRAMS dataset.

Table 2
Additional datasets: The number of chromosome images in training, validation, and test datasets in subsampled KIRAMS and KIRAMS + DIRAMS datasets.

	Subsampled KIRAMS dataset		KIRAMS + DIRAMS dataset	
	Normal	Dicentric	Normal	Dicentric
Training	2397	2397	112,922	11,670
Validation	266	266	12,547	1296
Test	5796	137	5796	137

four Geforce 1080 Ti GPUs with 11,264 MiB. The Tensorflow (2.8.0) [36] DL library and Python (3.8.10) were employed to utilize the modified DCNNs. The binary cross-entropy function was used as a loss function. A Bayesian optimization in Keras-tuner [37] was applied to search the optimal learning rates, batch sizes, dropout rates, and pooling layer types. The learning rate was sampled within the range of [5×10^{-7}, 5×10^{-4}], the dropout rate within the [0.0, 1.0], the pooling layer type from [global average pooling layer, max pooling layer], and the batch size within [32, 64, 96, 128, 160] with 200 maximum trial attempts. Each trial was carried out with 20 epochs. Both loss functions were minimized by an Adam optimizer with a decay rate of 10^{-6} and the suggested learning rate from the Keras-tuner. All layers in the pre-trained DCNNs were fine-tuned with 500 maximum epochs. An early stopping strategy was employed to complete the training when the validation loss did not decrease in 20 successive epochs. The weights of the fine-tuned DCNNs were stored when the validation loss was lowest during the training.

2.5. Evaluation metrics

Considering the class imbalance of normal chromosomes and DCs, it was necessary to calculate the accuracy of each class. Accordingly, true positive rate (TPR), true negative rate (TNR), positive predictive value (PPV), negative predictive value (NPV), and area under the receiver operating characteristic curve (AUROC) metrics were used to measure the performance of the DCNNs on the KIRAMS and DIRAMS datasets.

Positive values indicate DC cases and negative values indicate normal chromosome cases. The evaluated metrics, except AUROC, were defined by the following Eqs. (1)–(4).

$$\text{True positive rate: TPR} = \text{TP} / (\text{TP} + \text{FN}) \quad (1)$$

$$\text{True negative rate: TNR} = \text{TN} / (\text{TN} + \text{FP}) \quad (2)$$

$$\text{Positive predictive value: PPV} = \text{TP} / (\text{TP} + \text{FP}) \quad (3)$$

$$\text{Negative predictive value: NPV} = \text{TN} / (\text{TN} + \text{FN}) \quad (4)$$

where TP is the number of true positives, FN is the number of false negatives, TN is the number of true negatives, and FP is the number of false positives.

3. Results and discussion

The modified DCNNs were trained on a subsampled KIRAMS dataset, and another modified VGG19 was trained from scratch without transfer learning. The DCNNs were evaluated on the test KIRAMS dataset. The results of the modified DCNNs on the subsampled datasets are summarized in Table 3. The modified VGG19 achieved the best performance, with a TPR of 1.000, an NPV of 1.000, and an AUROC of 0.997. The modified DenseNet201 achieved the best performance, with a TNR of 0.966 and a PPV of 0.401. Therefore, the modified VGG19 was proposed as the baseline model because of its highest performance in TPR, NPV, and AUROC. The modified VGG19 without transfer learning exhibited a decrease in TPR, NPV, and AUROC by 0.036, 0.001, and 0.003, respectively, while showing an increase of 0.012 in TNR and 0.084 in PPV. Even though the use of transfer learning did not show significant performance improvements overall, it was employed in this study for training the model because of the performance enhancements in TPR, NPV, and AUROC.

The DC discrimination performances of our proposed model, the modified VGG19, trained on the KIRAMS datasets are summarized in Table 4. The modified VGG19 achieved a TPR of 0.927, a TNR of 0.997, a PPV of 0.882, an NPV of 0.998, and an AUROC of 0.997. Because the
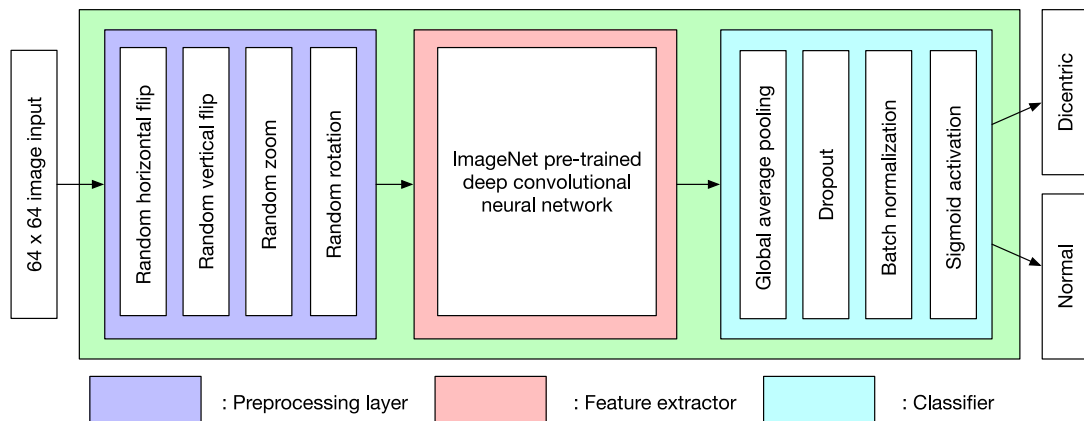

Fig. 2. Representative diagram of a modified DCNN.

Table 3

Comparison results of the DCNNs. The DCNNs were trained on the subsampled KIRAMS dataset.

Modified DCNN	TPR	TNR	PPV	NPV	AUROC
DenseNet121	0.993	0.951	0.324	1.000	0.995
DenseNet201	0.964	0.966	0.401	0.999	0.991
EfficientNetB5	0.949	0.944	0.286	0.999	0.979
EfficientNetB6	0.964	0.949	0.309	0.999	0.990
ResNet101	0.956	0.940	0.274	0.999	0.982
ResNet152	0.942	0.939	0.267	0.999	0.986
VGG16	0.993	0.945	0.299	1.000	0.997
VGG19	1.000	0.962	0.383	1.000	0.997
VGG19 (without transfer learning)	0.964	0.974	0.467	0.999	0.994

number of normal samples in the KIRAMS training dataset was 41 times higher than the number of normal samples in the subsampled KIRAMS dataset, the TPR was lower (0.920 vs. 1.000), but the PPV was significantly higher (0.882 vs. 0.383) than the results of the modified VGG19 trained on the subsampled KIRAMS dataset.

The performance results of the proposed model trained on the DIRAMS dataset are summarized in Table 5. The TPR, TNR, PPV, NPV, and AUROC were 0.991, 0.974, 0.966, 0.993, and 1.000 on the DIRAMS test dataset, respectively. The modified VGG19 was also evaluated on the test KIRAMS dataset. The modified VGG19 achieved a TPR of 0.993, a TNR of 0.858, a PPV of 0.145, an NPV of 1.000, and an AUROC of 0.983 on the test KIRAMS dataset.

The performance results of the proposed model trained on the KIRAMS + DIRAMS dataset are summarized in Table 6. The KIRAMS test dataset returned results with a TPR of 0.905, a TNR of 0.995, a PPV of 0.814, an NPV of 0.998, and an AUROC of 0.994, and the DIRAMS test dataset returned results with a TPR of 1.000, a TNR of 0.994, a PPV of 0.992, an NPV of 1.000, and an AUROC of 1.000. These results indicate that the proposed model was capable of DC discrimination on different datasets simultaneously.

The DC discrimination results of this and previous works are summarized in Table 7. Of note, the studies listed in Table 7 were conducted using different non-public datasets and input image types, metaphase spreads, and individual chromosome images; thus, the DC discrimination performance results were not directly comparable.

The DC discrimination capabilities of the chromosome classifiers in the models proposed by Rogan [3], Shen [7,10], Jang [8], Lorch [12], Room [14], and Li [17] might be limited due to the requirement to perform complex tasks, as they were programmed to detect and discriminate chromosomes using metaphase spread images.

Therefore, the emphasis was placed on the DC discrimination capability in this work, and chromosome detection and discrimination stages were separated, like Shen's approach [7,10]. Furthermore, manually labeled individual chromosome image data was utilized instead of automating chromosome detection. As a result, our proposed model could achieve high overall results because our model was able to focus solely on the DC discrimination task.

Figs. 3 and 4 demonstrate that our proposed model, as evaluated through the loss and TPR curves over multiple epochs, was successfully trained on the KIRAMS dataset. Additionally, the t-distributed stochastic neighbor embedding (t-SNE) method [38], a widely used technique for data clustering and visualization, was employed to visualize the chromosome image feature distribution obtained from the global average or

Table 4

Summary of the performance of modified VGG19s trained on the subsampled KIRAMS and KIRAMS training datasets and tested on the KIRAMS test dataset.

Training dataset	Test dataset	TPR	TNR	PPV	NPV	AUROC
Subsampled KIRAMS	KIRAMS	1.000	0.962	0.383	1.000	0.997
KIRAMS		0.927	0.997	0.882	0.998	0.997

Table 5

Performance results of the modified VGG19 trained on the DIRAMS training dataset and tested on the DIRAMS and KIRAMS test datasets.

Training dataset	Test dataset	TPR	TNR	PPV	NPV	AUROC
DIRAMS	DIRAMS	0.991	0.974	0.966	0.993	1.000
	KIRAMS	0.993	0.858	0.145	1.000	0.983

Table 6

Performance results of the modified VGG19 trained on the KIRAMS + DIRAMS train dataset and tested on the test dataset.

| Training dataset	Test dataset	TPR	TNR	PPV	NPV	AUROC
KIRAMS + DIRAMS	KIRAMS	0.905	0.995	0.814	0.998	0.994
	DIRAMS	1.000	0.994	0.992	1.000	1.000

Table 7

DC discrimination performances for our proposed models and the other studies (Note that the listed studies were conducted using different non-public datasets and input image type, and thus the dicentric chromosome discrimination performance results are not directly comparable.)

| Method	Input image type	TPR	TNR	PPV	NPV	AUROC
Classical machine learning method						
Rogan et al. [3]	Metaphase spreads	0.850	0.940	–	–	–
Shen et al. [7]		0.766	–	–	–	–
Lorch et al. [12]		0.039	0.910	0.444	0.996	–
Romm et al. [14]		0.536	0.998	0.823	0.994	–
Li et al. [17]		0.520	–	0.830	–	–
DL method						
Jang et al. [8]	Metaphase spreads	0.905	0.904	–	–	–
Shen et al. [10]		0.858	0.996	0.812	0.997	–
Proposed model (trained and tested on the DIRAMS dataset)	Individual chromosomes	0.991	0.974	0.966	0.993	1.000
Proposed model (trained and tested on the KIRAMS dataset)		0.927	0.997	0.882	0.998	0.997

max pooling layer of the proposed model. This method embeds higher-dimensional features onto lower-dimensional features while preserving the distances between adjacent features. In this way, such high-dimensional features can be visualized two dimensionally. The t-SNE visualization was performed on the modified VGG19 trained on both the DIRAMS and KIRAMS datasets. As illustrated in Figs. 5 and 6, blue and red points correspond to the test dataset's feature embeddings of normal chromosomes and DCs, respectively. These visualization results indicate that the image features of each class from each dataset, as processed by the modified VGG19, were effectively clustered.

4. Conclusion

In this study, a high-precision DC discrimination method using a modified and pre-trained VGG19 was proposed. This proposed method achieved high DC discrimination performance on both in vivo and ex vivo datasets. The results were as follows:
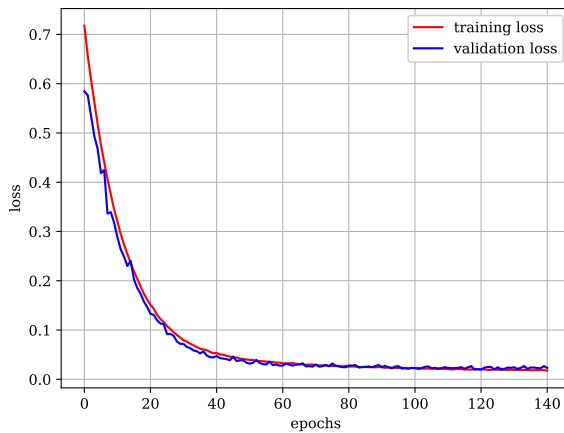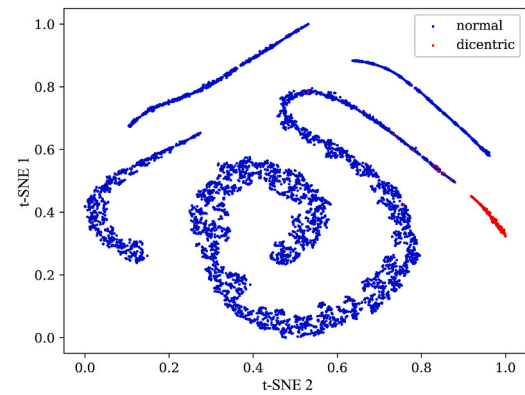
Fig. 3. Training and validation loss curves of the modified VGG19 on the KIRAMS datasets.
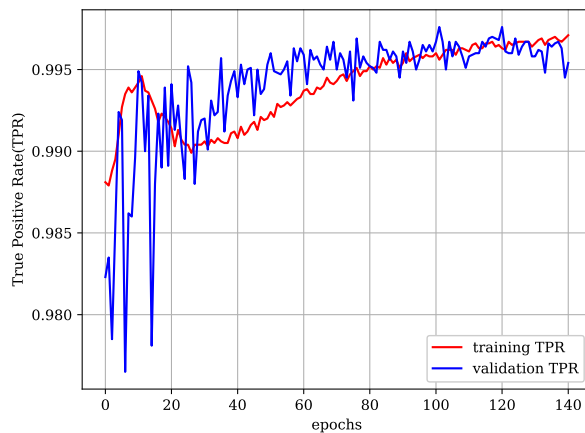
Fig. 4. TPR curves of the modified VGG19 on the KIRAMS training and validation datasets.
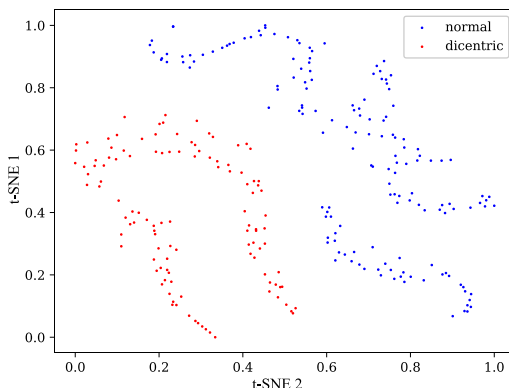
Fig. 5. t-SNE visualization of embedded image feature from the global average pooling layer of the modified VGG19 on the DIRAMS testing dataset.

Fig. 6. t-SNE visualization of embedded image feature from the max pooling layer of the modified VGG19 on the KIRAMS testing dataset.

(1) On the in vivo dataset, the proposed method achieved a TPR of 0.927, a TNR of 0.997, a PPV of 0.882, an NPV of 0.998, and an AUROC of 0.997.
(2) On the ex vivo dataset, the proposed method achieved a TPR of 0.991, a TNR of 0.974, a PPV of 0.966, an NPV of 0.993, and an AUROC of 1.000.

Our proposed model could be integrated into an end-to-end DC identification model that utilizes metaphase spread images as input.

Data availability statement

Due to privacy and ethical concerns, neither the data nor the source of the data can be made available.

Funding statement

Conflict of interest disclosure

The authors declare no potential conflict of interest.

Ethics approval statement

This research was approved by the Health Institutional Review Boards of our institution (IRB No. KIRAMS 2020-02-001)

References

[1] IAEA, Cytogenetic Dosimetry: Applications in Preparedness for and Response to Radiation Emergencies, International Atomic Energy Agency, 2011.
[2] C. Schunck, T. Johannes, D. Varga, T. Lörch, A. Plesch, New developments in automated cytogenetic imaging: unattended scoring of dicentric chromosomes, micronuclei, single cell gel electrophoresis, and fluorescence signals, Cytogenet. Genome Res. 104 (1–4) (2004) 383–389.
[3] P.K. Rogan, Y. Li, A. Wickramasinghe, A. Subasinghe, N. Caminsky, W. Khan, J. Samarabandu, R. Wilkins, F. Flegal, J.H. Knoll, Automating dicentric chromosome detection from cytogenetic biodosimetry data, Radiat Prot Dosimetry 159 (1–4) (2014) 95–104.
[4] B. Shirley, Y. Li, J.H.M. Knoll, P.K. Rogan, Expedited radiation biodosimetry by automated dicentric chromosome identification (ADCI) and dose estimation, J. Vis. Exp. 127 (2017).
[5] J. Liu, Y. Li, R. Wilkins, F. Flegal, J.H.M. Knoll, P.K. Rogan, Accurate cytogenetic biodosimetry through automated dicentric chromosome curation and metaphase cell selection, F1000Research 6 (2017) 1396.
[6] E. Royba, M. Repin, S. Pampou, C. Karan, D.J. Brenner, G. Garty, RABiT-II-DCA: a Fully-automated dicentric chromosome assay in Multiwell Plates, Radiat. Res. 192 (3) (2019) 311–323.
[7] X. Shen, Y. Qi, T. Ma, Z. Zhou, A dicentric chromosome identification method based on clustering and watershed algorithm, Sci. Rep. 9 (1) (2019) 2285.

[8] S. Jang, S.G. Shin, M.J. Lee, S. Han, C.H. Choi, S. Kim, W.S. Cho, S.H. Kim, Y. R. Kang, W. Jo, S. Jeong, S. Oh, Feasibility study on automatic Interpretation of radiation dose using deep learning technique for dicentric chromosome assay, Radiat. Res. 195 (2) (2021) 163–172.

[9] Y. Li, B.C. Shirley, R.C. Wilkins, F. Norton, J.H.M. Knoll, P.K. Rogan, Radiation dose estimation by completely automated Interpretation of the dicentric chromosome assay, Radiat Prot Dosimetry 186 (1) (2019) 42–47.

[10] X. Shen, T. Ma, C. Li, Z. Wen, J. Zheng, Z. Zhou, High-precision automatic identification method for dicentric chromosome images using two-stage convolutional neural network, Sci. Rep. 13 (1) (2023) 2124.

[11] G.M. Ludovici, M.G. Cascone, T. Huber, A. Chierici, P. Gaudio, S.O. de Souza, F. d'Errico, A. Malizia, Cytogenetic bio-dosimetry techniques in the detection of dicentric chromosomes induced by ionizing radiation: a review, The European Physical Journal Plus 136 (5) (2021) 482.

[12] T. Lorch, J. Bille, M. Frieben, G. Stephan, An Automated Biological Dosimetry System, Architectures and Algorithms for Digital Image Processing III, SPIE, 1986, pp. 199–206.

[13] J. Piper, J. Sprey, Adaptive classifiers for dicentric chromosomes, J. Radiat. Res. 33 (Suppl_1) (1992) 159–170.

[14] H. Romm, E. Ainsbury, S. Barnard, L. Barrios, J.F. Barquinero, C. Beinke, M. Deperas, E. Gregoire, A. Koivistoinen, C. Lindholm, J. Moquet, U. Oestreicher, R. Puig, K. Rothkamm, S. Sommer, H. Thierens, V. Vandersickel, A. Vral, A. Wojcik, Automatic scoring of dicentric chromosomes as a tool in large scale radiation accidents, Mutat. Res. 756 (1–2) (2013) 174–183.

[15] A.A. S, J. Samarabandu, J. Knoll, W. Khan, P. Rogan, An accurate image processing algorithm for detecting FISH Probe Locations relative to chromosome Landmarks on DAPI stained metaphase chromosome images, in: 2010 Canadian Conference on Computer and Robot Vision, 2010, pp. 223–230.

[16] A.S. Arachchige, J. Samarabandu, J.H. Knoll, P.K. Rogan, Intensity integrated Laplacian-based thickness measurement for detecting human metaphase chromosome centromere location, IEEE (Inst. Electr. Electron. Eng.) Trans. Biomed. Eng. 60 (7) (2013) 2005–2013.

[17] Y. Li, J.H. Knoll, R.C. Wilkins, F.N. Flegal, P.K. Rogan, Automated discrimination of dicentric and monocentric chromosomes by machine learning-based image processing, Microsc. Res. Tech. 79 (5) (2016) 393–402.

[18] A.S. Arachchige, J. Samarabandu, J. Knoll, W. Khan, P. Rogan, An image processing algorithm for accurate extraction of the centerline from human metaphase chromosomes, in: 2010 IEEE International Conference on Image Processing, IEEE, 2010, pp. 3613–3616.

[19] X. Bai, L.J. Latecki, W.-Y. Liu, Skeleton pruning by contour partitioning with discrete curve evolution, IEEE Trans. Pattern Anal. Mach. Intell. 29 (3) (2007) 449–462.

[20] A. Krizhevsky, I. Sutskever, G.E. Hinton, ImageNet classification with deep convolutional neural networks, in: Proceedings of the 25th International Conference on Neural Information Processing Systems - Volume 1, Curran Associates Inc., 2012, pp. 1097–1105.

[21] K. Simonyan, A. Zisserman, Very deep convolutional networks for large-scale image recognition, arXiv preprint arXiv:1409.1556 (2014).

[22] K. He, X. Zhang, S. Ren, J. Sun, Deep residual learning for image recognition, in: Proceedings of the IEEE Conference on Computer Vision and Pattern Recognition, 2016, pp. 770–778.

[23] G. Huang, Z. Liu, L. Van Der Maaten, K.Q. Weinberger, Densely connected convolutional networks, in: Proceedings of the IEEE Conference on Computer Vision and Pattern Recognition, 2017, pp. 4700–4708.

[24] M. Tan, Q. Le, Efficientnet: Rethinking model scaling for convolutional neural networks, in: International Conference on Machine Learning, PMLR, 2019, pp. 6105–6114.

[25] M.S. Al-Kharraz, L.A. Elrefaei, M.A. Fadel, Automated system for chromosome karyotyping to Recognize the Most Common Numerical Abnormalities using deep learning, IEEE Access 8 (2020) 157727–157747.

[26] W. Zhang, S. Song, T. Bai, Y. Zhao, F. Ma, J. Su, L. Yu, Chromosome classification with convolutional neural network based deep learning, 2018 11th international congress on image and signal processing, in: Biomedical Engineering and Informatics (CISP-BMEI), IEEE, 2018, pp. 1–5.

[27] Y. Wu, Y. Yue, X. Tan, W. Wang, T. Lu, End-to-end chromosome Karyotyping with data augmentation using GAN, in: 2018 25th IEEE International Conference on Image Processing (ICIP), IEEE, 2018, pp. 2456–2460.

[28] N. Xie, X. Li, K. Li, Y. Yang, H.T. Shen, Statistical Karyotype Analysis using CNN and Geometric optimization, IEEE Access 7 (2019) 179445–179453.

[29] C. Lin, G. Zhao, Z. Yang, A. Yin, X. Wang, L. Guo, H. Chen, Z. Ma, L. Zhao, H. Luo, T. Wang, B. Ding, X. Pang, Q. Chen, CIR-net: automatic classification of human chromosome based on Inception-ResNet Architecture, IEEE ACM Trans. Comput. Biol. Bioinf 19 (3) (2022) 1285–1293.

[30] M. Sharma, L. Vig, Automatic chromosome classification using deep attention based sequence learning of chromosome bands, in: 2018 International Joint Conference on Neural Networks (IJCNN), IEEE, 2018, pp. 1–8.

[31] G. Swati, M. Yadav, M. Sharma, L. Vig, Siamese networks for chromosome classification, in: 2017 IEEE International Conference on Computer Vision Workshops (ICCVW), 2017, pp. 72–81.

[32] S. Ren, K. He, R. Girshick, J. Sun, Faster r-cnn: towards real-time object detection with region proposal networks, Adv. Neural Inf. Process. Syst. 28 (2015).

[33] T.-Y. Lin, P. Dollár, R. Girshick, K. He, B. Hariharan, S. Belongie, Feature pyramid networks for object detection, in: Proceedings of the IEEE Conference on Computer Vision and Pattern Recognition, 2017, pp. 2117–2125.

[34] F. Chollet, Others, Keras, 2015.

[35] J. Deng, W. Dong, R. Socher, L.-J. Li, K. Li, L. Fei-Fei, Imagenet: a large-scale hierarchical image database, in: 2009 IEEE Conference on Computer Vision and Pattern Recognition, Ieee, 2009, pp. 248–255.

[36] A. Martín, A. Ashish, B. Paul, B. Eugene, C. Zhifeng, C. Craig, S.C. Greg, D. Andy, D. Jeffrey, D. Matthieu, G. Sanjay, G. Ian, H. Andrew, I. Geoffrey, I. Michael, Y. Jia, J. Rafal, K. Lukasz, K. Manjunath, L. Josh, M. Dandelion, M. Rajat, M. Sherry, M. Derek, O. Chris, S. Mike, S. Jonathon, S. Benoit, S. Ilya, T. Kunal, T. Paul, V. Vincent, V. Vijay, V. Fernanda, V. Oriol, W. Pete, W. Martin, W. Martin, Y. Yuan, Z. Xiaoqiang, TensorFlow: Large-Scale Machine Learning on Heterogeneous Systems, 2015.

[37] T. O'Malley, E. Bursztein, J. Long, F. Chollet, H. Jin, L. Invernizzi, Others, KerasTuner, 2019.

[38] G.E. Hinton, S. Roweis, Stochastic neighbor embedding, Adv. Neural Inf. Process. Syst. 15 (2002).